Journal Pre-proof

Uncovering the synergistic photocatalytic behavior of bimetallic molecular catalysts

Lin Yuan , Lei Zhang , Xiao-Xin Li , Jiang Liu , Jing-Jing Liu , Long-Zhang Dong , Dong-Sheng Li , Shun-Li Li , Ya-Qian Lan

Please cite this article as: Lin Yuan , Lei Zhang , Xiao-Xin Li , Jiang Liu , Jing-Jing Liu , Long-Zhang Dong , Dong-Sheng Li , Shun-Li Li , Ya-Qian Lan , Uncovering the synergistic photocatalytic behavior of bimetallic molecular catalysts, *Chinese Chemical Letters* (2022), doi: https://doi.org/10.1016/j.cclet.2022.01.039

Chinese Chemical Letters

journal homepage: www.elsevier.com

Uncovering the synergistic photocatalytic behavior of bimetallic molecular catalysts

Lin Yuan[a,†], Lei Zhang[b,†], Xiao-Xin Li[c], Jiang Liu[a,b,*], Jing-Jing Liu[b], Long-Zhang Dong[a], Dong-Sheng Li[d], Shun-Li Li[a,*], Ya-Qian Lan[a,b,*]

[a]*Jiangsu Collaborative Innovation Centre of Biomedical Functional Materials, Jiangsu Key Laboratory of New Power Batteries, College of Chemistry and Materials Science, Nanjing Normal University, Nanjing 210023, China.*
[b]*School of Chemistry, South China Normal University, Guangzhou 510006, China.*
[c]*School of Chemistry and Chemical Engineering, Southeast University, Nanjing 211189, China.*
[d]*Key Laboratory of Inorganic Nonmetallic Crystalline and Energy Conversion Materials, China Three Gorges University, Yichang 443002, China.*

Graphical Abstract
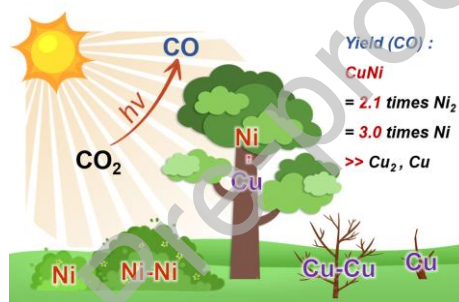
Design and construct a molecular model catalyst system (Ni-L^1, Cu-L^1, Ni$_2$-L^2, Cu$_2$-L^2 and CuNi-L^2) through regulating the metal sites (one or two, active or inactive) to study the improvement of photocatalytic CO_2RR efficiency caused by introducing the inactive metal ion.

ABSTRACT

Bimetallic catalysts usually exhibit better performance than monometallic catalysts due to synergistic effect. However, there is a lack of exploring the synergistic effect on catalytic performance caused by the introduction of inactive metal ion. In this work, we design a molecular model system that can precisely regulate the metal site number and catalytic property. When these molecular metal compounds are used as homogeneous catalysts for photocatalytic

---

∗ Corresponding author.
 E-mail address: yqlan@m.scnu.edu.cn

CO_2 reduction, the dinuclear heterometallic CuNi-L[2] shows the highest CO_2-to-CO conversion, which is 2.1 and 3.0 times higher than that of dinuclear homometallic Ni_2-L[2] and mononuclear Ni-L[1]. Density functional theory calculations demonstrate that, in CuNi-L[2], the introduction of inactive Cu^{II} is easier to promote the photo-generated electrons transferring to the coupled active Ni^{II} site to achieve the highest activity. In addition, this work also provides insights to design and construct more efficient bimetallic catalysts in future.

Photocatalytic CO_2 reduction reaction (CO_2RR) is one of the most promising and green methods of CO_2 conversion and utilization [1-4] for the reason that it can exploit solar energy as a driving force to convert low-value CO_2 into high-value carbon-based chemicals like CH_4, CO, CH_3OH, *etc.* [5-9]. At present, molecular metal compounds usually exhibit excellent photocatalytic performance such as high turnover number (TON) and turnover frequency (TOF) among the reported CO_2-photoreduction catalysts [10-12] due to the high active site utilization rate and the essence of homogeneous catalysis [13-16]. Particularly, the vast majority of molecular metal compounds can provide a clear single-crystal structure [17-19], allowing the catalytic active sites to be identified accurately and studying the reaction mechanism [20-22]. Based on these advantages [23], molecular metal compounds have the great potential to be used as model catalyst systems to understand the corresponding structure-property relationship [24-27], and thus guide for designing and synthesizing high-efficiency CO_2RR catalysts [28,29].

Generally, compared to monometallic catalysts, bimetallic catalysts always tend to show better performance in many catalytic reactions because of the synergistic effect of two interacted metal sites [30-34]. Unfortunately, only few suitable model systems were reported to specifically investigate the synergistic effect of two adjacent metal sites by means of second metal (activity or inactive) introduction on photocatalytic CO_2RR performance [35,36]. In many cases, metal ion-doping is the most common strategy used for surveying the influence of synergistic effect of two metal sites on the catalytic performance [37-39]. Although the ratio of two metal ions can be effectively adjusted by this method [40,41], it is hard to accurately control the position and coordination environment of the two specific metal ions [42,43], which affects the precise evaluation for the structure-property relationship [37]. In order to overcome this issue, the best way is to design and synthesize a well-defined model catalyst system that can accurately identify each catalytic site [44]. In the previous reports, only one molecular metal compound catalyst investigated the effect of the introduction of an inactive metal ion nearby active metal site on photocatalytic CO_2RR performance, but there are no direct interactions between the two involved metal sites [35]. If there are direct bonding interactions existed between two metal sites, the introduction of the secondary inactive metal site may significantly change the molecular orbitals and charge transfer characteristics of the active metal site, and thus affecting the final catalytic performance [45].

In light of these thoughts, a molecular metal compound model catalyst system including mononuclear [NiL[1](CH_3OH)] (labeled as Ni-L[1]), [CuL[1](H_2O)] (labeled as Cu-L[1]), dinuclear homometallic [Ni_2L[2](CH_3OH)$_2$] and [Cu_2L[2](CH_3OH)] (labeled as Ni_2-L[2] and Cu_2-L[2]), and dinuclear heterometallic [CuNiL[2]] (labeled as CuNi-L[2]) was designed and synthesized. Single crystal X-ray diffraction result shows that the Cu-L[1] and Ni-L[1] are isostructural, Ni_2-L[2], Cu_2-L[2] and CuNi-L[2] are isostructural. Importantly, these five molecular metal compounds can be regarded as a model catalyst system to systematically explore the influences of active monometallic site, bimetallic sites and heterometallic sites on the photocatalytic performance of CO_2RR in homogeneous conditions. The photocatalytic CO_2RR measurement results showed that both Ni-L[1] and Ni_2-L[2] exhibited high photocatalytic CO_2-to-CO activity, but neither Cu-L[1] nor Cu_2-L[2] showed catalytic activity, indicating that Ni^{II} is the photocatalytic active center while Cu^{II} is the inactive site. Moreover, under 8 h of visible light irradiation and the same concentration of Ni^{II} (0.8 μmol/L), the photocatalytic performance of Ni_2-L[2] (2.18 μmol) is better than that of Ni-L[1] (1.52 μmol), manifesting the dual active Ni^{II} sites show more advantageous catalytic activity owing to the synergistic effect. It is worth noting that for dinuclear heterometallic CuNi-L[2], the single active Ni^{II} site is coupled with inactive Cu^{II} ion, under the same photocatalytic conditions as Ni-L[1] and Ni_2-L[2], the CO yield of the photoreduced product is calculated to be 4.60 μmol (CO selectivity 93.5%), which is 2.1 and 3.0 times higher than that of Ni_2-L[2] and Ni-L[1], respectively. It reveals that the introduction of the secondary inactive Cu^{II} site can further promote the photocatalytic performance of the adjacent interacted active Ni^{II} ion. The density functional theory (DFT) calculation results declared that the electron cloud distribution around catalytic active site Ni^{II} ion is effectively enhanced owing to the introduction of relatively catalytic inactive Cu^{II} ion, which increases the electron-acquiring ability of active Ni^{II} site and significantly accelerates the photocatalytic CO_2RR. More

importantly, this work represents a well-defined model catalyst system to effectively reveal the important influence of the bimetallic synergy between active and inactive metal ions on the photocatalytic CO_2RR performance by adjusting the species, number and location of metal active centers in catalysts.

The CuNi-L^2 was synthesized through the precursor CuNa$_2$-L^2. A 50 mL EtOH solution of copper acetate (2.00 g, 0.01 mol) was slowly added to a 50 mL H$_2$O solution of H$_4$L^2 (3.84 g, 0.01 mol) and NaOH (0.8 g, 0.02 mol) [46,47]. The mixture was heated under reflux under N$_2$ atmosphere for 30 min followed by concentrating the resulting mixture to give a brown product CuNa$_2$-L^2 with quantitative yield. After acidification and recrystallization, crystal CuH$_2$-L^2 was obtained which further proved CuNa$_2$-L^2 synthesized successfully. Ni(ClO$_4$)$_2$·6H$_2$O (50 mg) and CuNa$_2$-L^2 (10 mg) was dissolved in 8 mL *N,N*-dimethylformamide (DMF) ultrasonically, then 2 mL EtOH was added into the solution. This solution was transferred into a 10 mL glass vial for 72 h at 353 K under autogenous pressure. After cooling down to room temperature, brown crystals were collected by filtration and fully washed with MeCN. The crystals were soaked in 20 mL of CH$_3$CN for 2 days replacing the solvent every 12 h. Finally, filtered and dried under vacuum. See supporting information for the specific synthesis methods of the other compounds.

Photocatalytic reduction of CO_2 was performed in a 50 mL quartz reactor with as-prepared crystals. Photocatalyst (0.02 μmol, Ni-L^1, Ni$_2$-L^2 and CuNi-L^2 based on the Ni^{II} site, Cu-L^1 and Cu$_2$-L^2 based on the Cu^{II} site), [Ru(bpy)$_3$]Cl$_2$·6H$_2$O (bpy = 2,2'-bipyridine, 0.02 mmol) were added into the mixed solution which contained CH$_3$CN (20 mL), H$_2$O (5 mL) and triisopropanolamine (TIPA, 5 mL) as an electron donor. After degassing with high-purity CO_2 to remove the dissolved O$_2$ for 30 min, the reaction was performed under the irradiation of a 300 W Xe lamp with UV-cut to keep the wavelengths in the range of exceeding 420 nm. The reaction temperature was kept at 298 K by using the cooling water circulation. In order to detect the content of reduction product produced by the reaction mixture, 500 μL of gas-product was extracted from the reactor with a syringe and injected into the GC equipped a flame ionization detector (FID) with a methanizer and a thermal conductivity detector (TCD), using nitrogen as the carrier gas. By comparing the integrated area of the gas-phase product with the calibration curve, the volume of carbon monoxide and hydrogen can be calculated. Each photocatalytic reaction was repeated at least three times to confirm the reliability of the data.

Single crystal X-ray diffraction result shows that the mononuclear Ni-L^1 crystallizes in triclinic system with the *P*-1 space group (Table S1 in Supporting information), and the asymmetric unit contains a transition metal ion Ni^{II}, a deprotonated Schiff base ligand (L^1)$^{2-}$ and a free methanol molecule. The only crystallographic Ni^{II} center is captured by the N$_2$O$_2$ chelating pocket (two N atoms from two C=N bonds and two O atoms from two phenolic hydroxyl groups) to form a planar quadrilateral coordination configuration. It is noteworthy that the Ni^{II} ion and its coordination atoms in Ni-L^1 are totally in the same plane. This means that there is sufficient coordination space in axial position of the metal ion to allow small molecules to attack. Moreover, the Ni^{II} ion in Ni-L^1 can be replaced by Cu^{II} ion, namely the isostructural Cu-L^1, which crystallizes in the orthorhombic system with a *Pnma* space group (Table S1). In addition, we further introduced carboxyl groups in the *ortho* positions of the two phenolic hydroxyl groups of H$_2$L^1 to synthesize the H$_4$L^2 ligand containing two metal ion chelating pockets (N$_2$O$_2$ and O$_4$ coordination modes). The ligand can catch hold of two identical or different metal ions effectively. Furthermore, just like the original N$_2$O$_2$ cavity, all coordination atoms of the constructed parallel secondary O$_4$ coordination mode are also composed of a planar quadrilateral geometry. When the H$_4$L^2 ligand captures two Ni^{II} ions, a dinuclear homometallic compound Ni$_2$-L^2 is synthesized and it crystallizes in triclinic system with the space group *P*-1 (Table S2 in Supporting information). Ni1 atom is located in N$_2$O$_2$ chelating pocket, while Ni2 atom is captured by another O$_4$ chelating pocket. Ni1 and Ni2 atoms are connected and interacted with each other by sharing two phenolic hydroxyl O atoms. Similarly, the H$_4$L^2 ligand can also clamp two Cu^{II} ions to form an isostructural homometallic Cu$_2$-L^2, but which crystallizes in monoclinic system with the *P*2$_1$/*c* space group (Table S2). More importantly, we can fix Cu^{II} and Ni^{II} ions simultaneously by these two kinds of different chelating pockets of H$_4$L^2 ligand though stepwise synthesis method to construct isostructural dinuclear heterometallic compound CuNi-L^2, which crystallizes in monoclinic system with *C*2/*c* space group (Table S2). For CuNi-L^2, Cu1 atom is trapped into the N$_2$O$_2$ chelating pocket, and Ni1 atom is fastened by the O$_4$ coordination mode. It is worth noting that due to the similar configuration of these compounds, this series of compounds Ni-L^1, Cu-L^1, Ni$_2$-L^2, Cu$_2$-L^2 and CuNi-L^2 (Fig. 1) can serve as model systems to study the effects of monometallic, bimetallic (homometallic and heterometallic) compounds on the catalytic performance for specific small molecule activity. More importantly, the performance impact produced by the synergistic effect between dinuclear metal ions can be explored systematically.
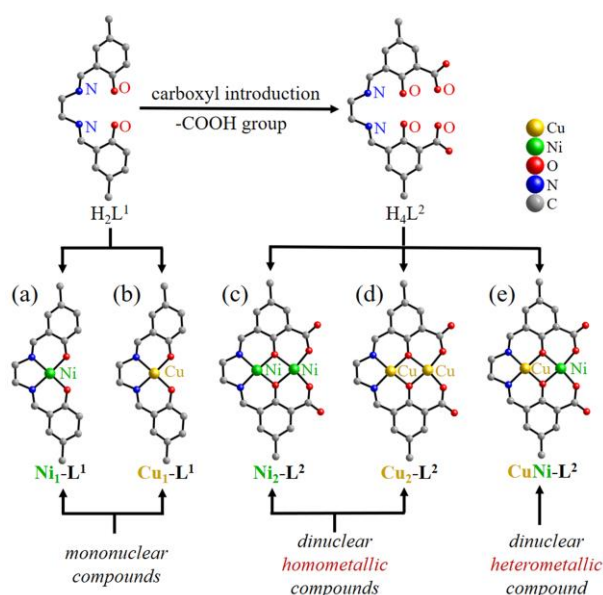
Fig. 1. Structures of the molecular complexes. (a) mononuclear Ni-L¹; (b) mononuclear Cu-L¹; (c) dinuclear Ni₂-L²; (d) dinuclear Cu₂-L²; (e) dinuclear CuNi-L². All hydrogen atoms are omitted for clarity. Cu, yellow; Ni, green; O, red; N, blue; C, gray.

The phase purity of Ni-L¹, Cu-L¹, Ni₂-L², Cu₂-L² and CuNi-L² were confirmed by well-matched powder X-ray diffraction (PXRD) patterns (Figs. S1-S5 in Supporting information). According to the X-ray photoelectron spectroscopy (XPS) and inductively coupled plasma optical emission spectrometer (ICP-OES) results (Table S3 in Supporting information), the valence of Ni and Cu is +2 (Fig. 2a and Fig. S6 in Supporting information) and the stoichiometric ratio of Cu/Ni in CuNi-L² is 1:1. Furthermore, the thermogravimetric analysis (TGA) curves of Ni-L¹, Cu-L¹, Ni₂-L², Cu₂-L² and CuNi-L² showed that their structures can be maintained well below 300 °C under air atmosphere (Fig. S7 in Supporting information). To evaluate the potential of the five compounds as photocatalysts, we performed a series of characterizations to assess their band structures. The Highest Occupied Molecular Orbital (HOMO) positions of the five molecular compounds were evaluated approximately by cyclic voltammetry (CV) (Fig. 2b, Figs. S13-S16 in Supporting information). Thus, the HOMO energy levels of the compounds were estimated to be 6.59 eV (1.74 V *vs.* NHE), 6.73 eV (1.88 V *vs.* NHE), 6.63 eV (1.78 V *vs.* NHE), 6.77 eV (1.92 V *vs.* NHE), 6.40 eV (1.55 V *vs.* NHE) for Ni-L¹, Cu-L¹, Ni₂-L², Cu₂-L² and CuNi-L², respectively. The bandgaps (E_g) of Ni-L¹, Cu-L¹, Ni₂-L², Cu₂-L² and CuNi-L² were estimated by the UV-vis absorption spectra (Fig. 2c). The E_g values were calculated to be 2.36, 2.51, 2.46, 2.51 and 2.17 eV, respectively. Then the Lowest Unoccupied Molecular Orbital (LUMO) positions of Ni-L¹, Cu-L¹, Ni₂-L², Cu₂-L² and CuNi-L² were calculated to be − 0.62 V, −0.63 V, −0.68 V, −0.59 V, −0.62 V *vs.* NHE, pH 7. As the LUMO positions of these compounds are more negative than the redox potentials of most photocatalytic CO₂RR products such as HCOOH (−0.58 V *vs.* NHE, pH 7), CO (−0.51 V *vs.* NHE, pH 7) or CH₄ (−0.24 V *vs.* NHE, pH 7) (Fig. 2d), these compounds have potential for CO₂RR as catalysts [48].
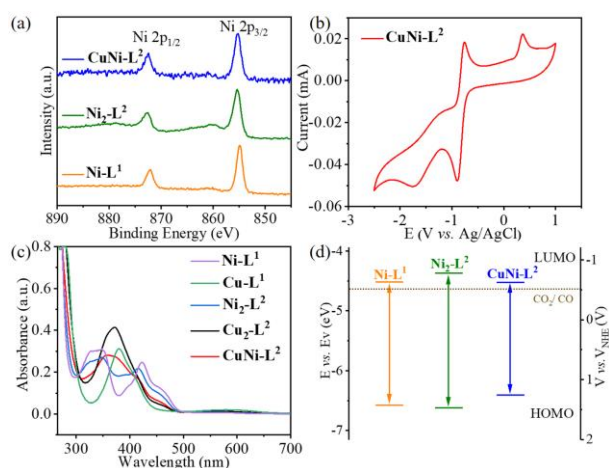
Fig. 2. (a) High resolution Ni 2p XPS spectra of Ni-L^1, Ni$_2$-L^2 and CuNi-L^2 in survey scan. (b) Cyclic voltammogram of CuNi-L^2 in acetonitrile containing 0.1 mol/L Bu$_4$NPF$_6$ at a scan rate of 50 mV/s. (c) UV-vis absorption spectra of Ni-L^1, Cu-L^1, Ni$_2$-L^2, Cu$_2$-L^2 and CuNi-L^2 in the solution state (chloroform). (d) Band structure for Ni-L^1, Ni$_2$-L^2 and CuNi-L^2.

Taking all the above features into consideration, the photocatalytic CO_2RR of these compounds as homogeneous catalysts were tested under a pure atmosphere of CO_2 (1.0 atm, 25 °C) in a 30 mL CH_3CN/H_2O solution (v/v = 4:1) with a certain amount (0.8 μmol/L) of catalysts, triisopropanolamine (TIPA) as electron donor and [Ru(bpy)$_3$]Cl$_2$·6H$_2$O as auxiliary photosensitizer (PS) under visible light irradiation (λ ≥ 420 nm) [11,49]. After being irradiated, the generated gases products were analyzed by gas chromatography (GC) (Fig. S17 in Supporting information) and the liquid products were tested by Nuclear Magnetic Resonance (NMR). The results showed that the main gaseous reductive products of these compounds were CO and H_2, and no liquid reduction products were detected in the reaction system. As the irradiation time increased, the reduction products decreased gradually per unit time, and there is almost no product generating after 8 h. After one single photoredox cycle, 1.52 μmol of CO and 0.20 μmol of H_2 were produced in accordance with a CO selectivity of 88.4% and a TON$_{CO}$ of 76 catalyzed by mononuclear compound Ni-L^1 (0.8 μmol/L) within 8 h. In contrast, as the catalyst replaced by another mononuclear compound Cu-L^1, almost no reduction products were detected. This consequence implied that the metal ion Cu^{II} is inactive in this catalytic system. Specifically, when the photocatalyst changed from the mononuclear complex Ni-L^1 to the bimetallic complex Ni$_2$-L^2 (0.4 μmol/L) with the same Ni^{II} ion concentration and irradiation time, the yield of CO was increased to 2.18 μmol (TON = 109), along with the selectivity of CO was also improved from 88.4% to 93.9% (Fig. 3a). The results showed that both of the Ni^{II} ions in the two types of coordination environment (N$_2$O$_2$ and O$_4$) have effective photocatalytic CO_2RR capabilities. There is no doubt that introducing the second metal has a certain positive effect on the product selectivity. However, the isomorphic compound Cu$_2$-L^2 produced only trace amounts of gaseous products, which confirmed that Cu^{II} ion expresses negligible catalytic activity in this photocatalytic system one step closer. In other words, Cu^{II} ion did not show an effective photocatalytic CO_2 reduction ability whether it was in the N$_2$O$_2$ coordination environment or the O$_4$ coordination environment. Interestingly, when CuNi-L^2 (0.8 μmol/L) acted as the catalyst, it showed the highest CO yield (4.60 μmol) among the nickel-containing catalysts (Ni-L^1, Ni$_2$-L^2 and CuNi-L^2) under the identical photocatalytic condition. The TON$_{CO}$ was up to 230, which was 2.1 and 3.0 times as much as that of Ni$_2$-L^2 and Ni-L^1 respectively. Meanwhile, the selectivity for CO was 93.5%, which was comparable to that of Ni$_2$-L^2. A summary of the specific selectivities, TONs and TOFs of these photocatalytic systems were provided in Table S4 (Supporting information).

Considering that CuNi-L^2 presented the highest photocatalytic activity and superior selectivity for CO_2-to-CO conversion, a collection of control tests with CuNi-L^2 as the representative example were carried out to identify the roles of catalyst and other influence factors in photocatalytic CO_2RR. The corresponding results were summarized in Table S4. No gas phase product was detected when the photocatalytic reaction was performed without CO_2 (replaced by N_2) (Table S4, entry 4), which indicated the detected CO originated from CO_2. The absence of gas production in the dark indicated that it is the truly

photoexcited states to initiate the reaction (Table S4, entry 5). Moreover, the reaction system in the absence of TIPA exhibited trace evolution amount of CO, suggesting that the photoexcited states of CuNi-L^2 were reductively quenched by TIPA (Table S4, entry 6). When the photocatalytic system without CuNi-L^2 or photosensitizer, a trace amount of CO was detected (Table S4, entries 7 and 8). The above experimental results showed that the catalyst, photosensitizer, visible light, CO_2 atmosphere and TIPA are all the indispensable reaction conditions in this photocatalytic CO_2RR model system. At the same time, noting that CO production was also very low in the absence of H_2O (Table S4, entry 9), we conducted a series of experiments to explore the influence of different proportions of H_2O on CO_2RR. When the ratio of H_2O/CH_3CN was slightly increased to 1:9, the yield of CO (3.7 µmol) was increased significantly, indicating that H_2O acted as an important proton source in the reaction process. When the H_2O/CH_3CN ratio further increased to 1:4, the amount of CO was increased to 4.6 µmol, and the selectivity was also risen from 77.1% to 91.3% at the same time. However, as the H_2O/CH_3CN ratio reached to 1:1, the yield of CO decreased instead, and only a few CO produced in pure H_2O (Table S5 in Supporting information).

After an 8-h photocatalysis, the total amount of gaseous products produced hardly increased (Fig. 3b), which may attribute to the inactivation of the photosensitizer. In order to confirm that, recycling experiments were carried out by taking CuNi-L^2 as an example. When almost no CO was produced after being illuminated for 8 h, the equal amounts of fresh PS was added into the system and pure CO_2 gas was reintroduced. As expected, the stagnated reaction was activated again, which indicated that the termination of the system results from the deactivation of the photosensitizer rather than the poisoning of CuNi-L^2 catalyst. Moreover, CuNi-L^2 completed at least three cycles of 8 h reaction with a high total CO output (9.23 µmol) and fine selectivity (91.6%) to CO (Fig. 3c). Additionally, the apparent quantum efficiency (AQE) of CuNi-L^2, Ni_2-L^2 and Ni-L^1 were also measured under the monochromatic light of 420 nm (see Supporting information). The corresponding results showed that the ϕ_{CO} of CuNi-L^2 was calculated to be 0.018%, which was 2-fold higher than Ni_2-L^2 (0.0086%) and around 3-fold higher than Ni-L^1 (0.0060%). In order to confirm that the produced CO indeed comes from CO_2 reduction, isotopic tracing experiment was performed with representative CuNi-L^2 catalyst in $^{13}CO_2$ atmosphere. After irradiation under visible light for 4 h, gas chromatography-mass spectrometry (GC-MS) was used to analyze the reaction products. The detected peak of m/z 29 was assigned to ^{13}CO, the peaks of m/z 13 and 16 belong to the debris of ^{13}C and ^{16}O (Fig. 3d). It is clear from the result that ^{13}CO was converted from the $^{13}CO_2$ atmosphere, which indicated that CO is derived from the photocatalytic CO_2 reduction instead of the compounds decomposing (catalyst/PS/TIPA) in the catalytic system. At the same time, the ^{13}C NMR spectrum indicated that there were no liquid reduction products detected in a series of reactions above (Fig. S20 in Supporting information) [50,51]. As a result, this fact proved that the catalysts had good selectivity, and it also demonstrated that these compounds did have the CO_2RR activity. In addition, the steady-state photoluminescence (PL) spectroscopy of CuNi-L^2 was further carried out to provide insight into the excited states recombination behavior (Fig. S21 in Supporting information). It can be observed that the fluorescence intensity decreases gradually as the catalyst concentration increases, indicating that CuNi-L^2 has a good separation efficiency of photogenerated carriers. Based on the above photocatalytic tests, both the mononuclear compound Ni-L^1 and the dinuclear compound Ni_2-L^2 showed high CO_2RR performance, indicating that the Ni^{II} ions in the two coordination environments (N_2O_2 and O_4) possess effective catalytic activities. Moreover, Ni_2-L^2 exhibits better catalytic ability than Ni-L^1 under the same Ni^{II} ion concentration, we guess that it may be caused by the certain metal synergistic catalysis between the two Ni^{II} sites in different coordination environments. However, when the catalyst was replaced by the isomorphic Cu-L^1 and Cu_2-L^2 respectively, they did not show effective photocatalytic activity. That is to say, the Cu^{II} ions in the two coordination environments hardly express photocatalytic performance. It is worth noting CuNi-L^2 involves one active site Ni^{II}, but it shows the highest catalytic activity among these five catalysts. We considered that the inactive Cu^{II} ion probably exerts a certain effect on improving the photocatalytic activity of neighboring active Ni^{II} site.
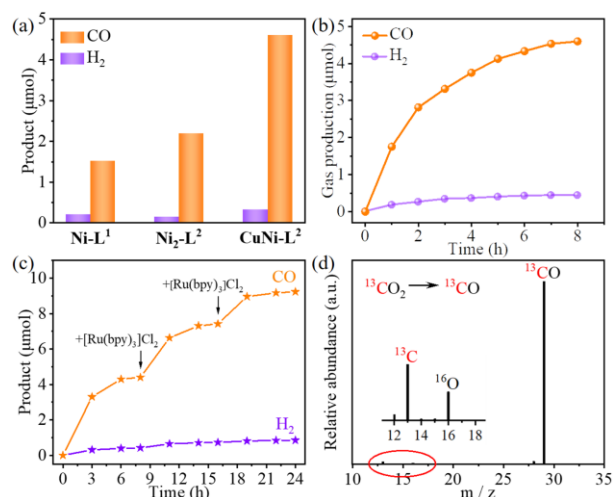
Fig. 3. The photocatalytic CO_2RR was carried out under the conditions of a 30 mL CO_2-saturated CH_3CN/H_2O solution (v/v = 4:1) at 25 °C with the same concentration of Ni^{II} (0.8 μmol/L), TIPA (0.8 mol/L) and $[Ru(bpy)_3]Cl_2·6H_2O$ (0.85 mmol/L) under visible light irradiation (λ ≥ 420 nm, irradiation area, 7.06 cm^2). (a) Photocatalytic production of CO and H_2 catalyzed by Ni-L^1 (0.8 μmol/L), Ni$_2$-L^2 (0.4 μmol/L) and CuNi-L^2 (0.8 μmol/L). (b) Mounts of CO and H_2 produced as a function of the visible-light irradiation time over CuNi-L^2 (0.8 μmol/L). (c) Durability test for CuNi-L^2 (0.8 μmol/L). (d) The mass spectra of ^{13}CO recorded under a $^{13}CO_2$ atmosphere.

The experimental results demonstrated that the photocatalytic CO_2RR activities of the five monomolecular compounds gradually decreased by CuNi-L^2, Ni$_2$-L^2, Ni-L^1, Cu$_2$-L^2 and Cu-L^1 successively. DFT calculation was employed to get insight into the activity of the photocatalytic conversion of CO_2-to-CO. Then the Gibbs free energy (G) of the CO_2RR paths are compared to explore the differences in photocatalytic activity of the five catalysts (Fig. 4a). The CO_2-to-CO reduction pathway is primarily composed of three steps: CO_2 activation and hydrogenation (CO_2 → *COOH), dehydration (*COOH → *CO), and CO desorption (*CO → CO), where the rate-determining step is the first path. The energy change from CO_2 to *COOH on CuNi-L^2 and Ni$_2$-L^2 are the lowest (0.81 eV and 0.85 eV), Ni-L^1 (1.44 eV), Cu$_2$-L^2 (1.57 eV) and Cu-L^1 (1.97 eV), suggesting the highest activity of dual TM centers (CuNi-L^2 and Ni$_2$-L^2) for CO_2 reduction. For the two investigated transitional metal ions, Cu^{II} sites apparently present an inactive behavior for the CO_2RR due to large energy increase for the formation of *COOH. Although the above results are consistent with the photocatalytic activity of the catalysts, the energy change from CO_2 to *COOH of CuNi-L^2 is not far different from Ni$_2$-L^2, while the CO production of CuNi-L^2 is about 1.5 times than that of Ni$_2$-L^2 in experiment. The dual TM sites were expected to stabilize the *COOH intermediate with a bridge structure, but the adsorbate returns to a single Ni^{II} site after geometry optimization (Fig. S22 in Supporting information). That is to say, the coordination environment of the Ni^{II} ions is crucial during the photocatalytic possess. In order to further explore the structure-activity relationship between CuNi-L^2 and Ni$_2$-L^2, time-dependent DFT calculations were performed to investigate the excitation properties of CuNi-L^2 and Ni$_2$-L^2 systems. Fig. 4b illustrates the electron contributions of the first excited state, which is basically contributed by HOMO-LUMO transition, the charge density difference between the ground state (S_0) and the first excited state (S_1). It is clear from the result above that the excited electron of Ni$_2$-L^2 is concentrated around two Ni^{II} ions and the coordinated N, O atoms, while the electron of CuNi-L^2 is mainly concentrated on the Ni^{II} ion and O atoms, no electron accumulates around the Cu^{II} ion and N atoms. In addition, the charge analysis reveals that the charge transfer from Ni^{II} ions to N_2O_2 and O_4 coordination are 0.21 and 0.47 respectively (Fig. 4c), indicating that Ni^{II} ions in the two coordination environments both have good reduction ability, of which the Ni^{II} in O_4 coordination possesses better reduction activity. Meanwhile, comparing the free energy change between the two Ni^{II} sites, the Ni^{II} in O_4-coordination expresses a lower energy change from CO_2 to *COOH than Ni^{II} in N_2O_2 coordination environment, which further proves the result above. The charge transfer in CuNi-L^2 for metal ions are 0.65 (Ni^{II}) and 0.01 (Cu^{II}) respectively. It can be found that the existence of inactive Cu^{II} ion promotes the accumulation of electrons on Ni^{II}, which causes the Ni^{II} with O_4 coordination environment in CuNi-L^2 expressing better reduction

ability than that of Ni_2-L^2, and then significantly accelerates the photocatalytic reduction reaction of CO_2 to CO.

According to the above DFT calculation results, the corresponding photocatalytic CO_2RR mechanism can be proposed (Fig. 4d). Firstly, $[Ru(bpy)_3]Cl_2 \cdot 6H_2O$ is excited by the irradiation of visible light. Since the LUMO positions of the five compounds are lower than that of $[Ru(bpy)_3]Cl_2 \cdot 6H_2O$, the photo-generated electrons can be transferred to the catalysts. At the same time, CO_2 molecules are adsorbed and activated by the exposed metal sites of the catalysts. Secondly, the adsorbed CO_2 on the active metal center obtains an electron and a proton to form a *COOH intermediate. Next, the *COOH intermediate gets an electron and a proton, then the *CO species is generated after dehydration from the *COOH. Finally, CO is generated by the desorption of *CO separating from the surface of the catalysts. The sacrificial electron donor was performed by TIPA to fill the holes and reductive quench the excited photosensitizer. The catalysts regenerated and enter the next cycle of CO_2-to-CO conversion.
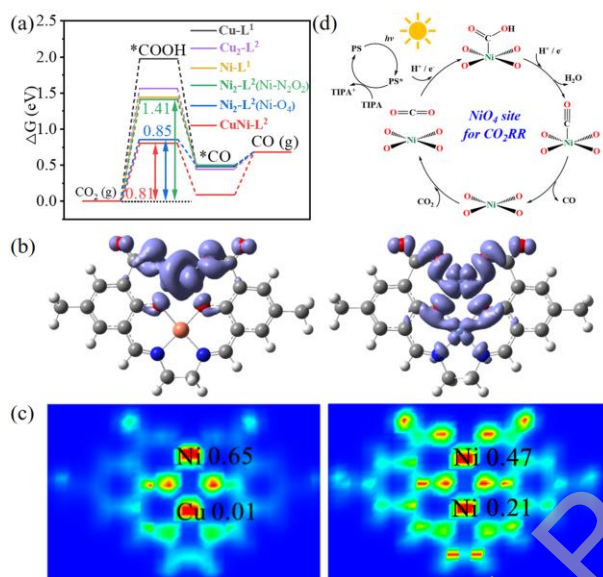

Fig. 4. (a) The free-energy profile for the CO_2RR pathway. (b) Charge density difference plot for the first excited state of $CuNi-L^2$ (left) and Ni_2-L^2 (right). (c) 2D display of charge density of $CuNi-L^2$ (left) and Ni_2-L^2 (right) systems. (d) Proposed photocatalytic mechanism of the molecular metal compounds for the CO_2 to CO conversion.

In summary, we design and synthesize five molecular metal compounds, containing mononuclear $Ni-L^1$ and $Cu-L^1$, dinuclear homometallic Ni_2-L^2, Cu_2-L^2 and dinuclear heterometallic $CuNi-L^2$. These molecular metal compounds can be regarded as a model catalyst system to systematically probe the influence on photocatalytic CO_2RR performance caused by monometallic site, bimetallic sites and heterometallic sites by precisely controlling of the species, number and catalytic properties of metal ion centers. In particular, it explores the direct effect of introducing inactive metal ions into bimetallic catalysts on the photocatalytic CO_2RR performance of two neighboring metal centers. When these molecular metal compounds act as homogeneous catalysts, the inactive Cu-introduced dinuclear heterometallic $CuNi-L^2$ (0.8 µmol/L) exhibits the highest photocatalytic selectivity (93.5%) and activity (4.60 µmol) after an 8-h photocatalysis, which is 2.1 and 3.0 times than that of dinuclear homometallic catalyst Ni_2-L^2 (2.18 µmol) and the mononuclear catalyst $Ni-L^1$ (1.52 µmol) respectively with the same concentration of Ni^{II} (0.8 µmol/L). The related DFT calculation results also show that, compared with Ni_2-L^2, the photo-generated electrons in $CuNi-L^2$ are promoted transferring to the adjacent active Ni^{II} site due to the introduction of inactive Cu^{II} ion. This fact improves the utilization efficiency of photo-generated electrons, and then the photocatalytic CO_2RR activity of Ni^{II} ions. Significantly, more insights were provided by this work for the future design and construction of high-efficiency bimetallic photocatalysts applied to photocatalytic CO_2RR.

Declaration of competing interest

The authors report no declarations of interest.

Acknowledgment

References

[1] X. Chang, T. Wang, P. Yang, G. Zhang, J. Gong, Adv. Mater. 31 (2019) 1804710.
[2] Y. Hu, F. Zhan, Q. Wang, et al., J. Am. Chem. Soc. 142 (2020) 5618-5626.
[3] M. Sun, C. Wang, C.Y. Sun, et al., J Catal. 385 (2020) 70-75.
[4] S. Navarro-Jaén, M. Virginie, J. Bonin, et al., Nat. Rev. Chem. 5 (2021) 564-579.
[5] W. Tu, Y. Zhou and Z. Zou, Adv. Mater. 26 (2014) 4607-4626.
[6] Y. Wang, N.Y. Huang, J.Q. Shen, et al., J. Am. Chem. Soc. 140 (2018) 38-41.
[7] H. Zhong, R. Sa, H. Lv, et al., Adv. Funct. Mater. 30 (2020) 2002654.
[8] M. Ding, H.L. Jiang, ACS Catal. 8 (2018) 3194-3201.
[9] H. Rao, L. C. Schmidt, J. Bonin, M. Robert, Nature 548 (2017) 74-77.
[10] D. Mellmann, P. Sponholz, H. Junge, M. Beller, Chem. Soc. Rev. 45 (2016) 3954-3988.
[11] P. Wang, R. Dong, S. Guo, et al., Nat. Sci. Rev. 7 (2020) 1459-1467.
[12] Z. Guo, S. Cheng, C. Cometto, et al., J. Am. Chem. Soc. 138 (2016) 9413-9416.
[13] Q. Fu and C. Draxl, Phys. Rev. Lett. 122 (2019) 046101.
[14] T. Ouyang, H.H. Huang, J.W. Wang, D.C. Zhong, T.B. Lu, Angew. Chem. Int. Ed. 56 (2017) 738-743.
[15] V. S. Thoi, N. Kornienko, C. G. Margarit, P. Yang, C. J. Chang, J. Am. Chem. Soc. 135 (2013) 14413-14424.
[16] T. Ishizuka, A. Watanabe, H. Kotani, et al., Inorg. Chem. 55 (2016) 1154-1164.
[17] L. Zhang, X.X. Li, Z.L. Lang, et al., J. Am. Chem. Soc. 143 (2021) 3808-3816.
[18] N. Li, J. Liu, B.X. Dong, Y.Q. Lan, Angew. Chem. Int. Ed. 59 (2020) 20779-20793.
[19] L. Ma, Q. Wang, W.L. Man, et al., Angew. Chem. Int. Ed. 54 (2015) 5246-5249.
[20] L.Z. Dong, L. Zhang, J. Liu, et al., Angew. Chem. Int. Ed. 59 (2020) 2659-2663.
[21] Z.-H. Yan, M.H. Du, J. Liu, et al., Nat. Commun. 9 (2018) 3353.
[22] D. Hong, Y. Tsukakoshi, H. Kotani, T. Ishizuka, T. Kojima, J. Am. Chem. Soc. 139 (2017) 6538-6541.
[23] N. Elgrishi, M. B. Chambers, X. Wang, M. Fontecave, Chem. Soc. Rev. 46 (2017) 761-796.
[24] J.J. Liu, N. Li, J.W. Sun, et al., ACS Catal. 11 (2021) 4510-4519.
[25] N. Bakharev, D. Bono, H. B. Brom, et al., Phys. Rev. Lett. 96 (2006) 117002.
[26] N. Zheng, X. Bu, P. Feng, J. Am. Chem. Soc. 124 (2002) 9688-9689.
[27] H. Rao, J. Bonin and M. Robert, ChemSusChem. 10 (2017) 4447-4450.
[28] H.X. Zhang, Q.L. Hong, J. Li, et al., Angew. Chem. Int. Ed. 58 (2019) 11752-11756.
[29] X.X. Li, L. Zhang, J. Liu, et al., JACS Au. 1 (2021) 1288-1295.
[30] Y. Chen, S. Fan, B. Qiu, et al., ACS Appl. Mater. Interfaces 13 (2021) 24795-24803.
[31] B. Guo, Q. Li, J. Lin, et al., ACS Appl. Nano Mater. 4 (2021) 1849-1857.
[32] Kashid, D. J. Patil, R. D. Mali, et al., Catal Letters. 151 (2021) 353-358.
[33] C. Liu, C.L. Ji, T. Zhou, X. Hong, M. Szostak, Angew. Chem. Int. Ed. 60 (2021) 10690-10699.
[34] J. Xu, Z. Ju, W. Zhang, et al., Angew. Chem. Int. Ed. 60 (2021) 8705-8709.
[35] T. Ouyang, H.J. Wang, H.H. Huang, et al., Angew. Chem. Int. Ed. 57 (2018) 16480-16485.
[36] S.M. Liu, Z. Zhang, X. Li, et al., Adv. Mater. Interfaces 5 (2018) 1801062.
[37] J. Z. Bloh, R. Dillert, D. W. Bahnemann, J. Phys. Chem. C 116 (2012) 25558-25562.
[38] X. Feng, F. Pan, H. Zhao, et al., Appl. Catal. B 238 (2018) 274-283.
[39] Z. Jiang, J. Liu, M. Gao, et al., Adv. Mater. 29 (2017) 1603369.
[40] B. Tang, X. Yang, Z. Kang, L. Feng, Appl. Catal. B 278 (2020) 119281.
[41] B. Liu, Y.F. Zhao, H.Q. Peng, et al., Adv. Mater. 29 (2017) 1606521.
[42] Z. Li, H. Dong, Y. Zhang, et al., J. Phys. Chem. C 112 (2008) 16046-16051.
[43] B. Zhang, J. Zhang, F. Zhang, et al., Adv. Funct. Mater. 30 (2020) 1906194.
[44] L. Feng, K.Y. Wang, E. Joseph, H.C. Zhou, Trends Chem. 2 (2020) 555-568.
[45] S. N. Habisreutinger, L. Schmidt-Mende, J. K. Stolarczyk, Angew. Chem. Int. Ed. 52 (2013) 7372-7408.
[46] J. P. Beale, J. A. Cunningham, D. J. Philips, Inorg. Chim. Acta. 33 (1979) 113–118.
[47] N. Pilkington, R. Robson, Aust. J. Chem. 23 (1970) 2225-2236.
[48] X. Chang, T. Wang, J. Gong, Energy Environ. Sci. 9 (2016) 2177-2196.
[49] X.K. Wang, J. Liu, L. Zhang, et al., ACS Catal. 9 (2019) 1726-1732.
[50] Y. Fu, D. Sun, Y. Chen, et al., Angew. Chem. Int. Ed. 51 (2012) 3364-3367.
[51] N. Li, J.J. Liu, J.W. Sun, et al., Green Chem. 22 (2020) 5325-5332.